 CMC, vol.2, no.3, pp.151-162, 2005

# Stability of Solder Bridging for Area Array Type Packaging

**Wen-Hwa Chen [1,2], Shu-Ru Lin [2] and Kuo-Ning Chiang [2, 3]**

**Abstract:** As ultra-fine-pitch technologies are adopted to enhance the performance of electronic packaging, solder bridging becomes an urgently serious defect. This work presents a computational model using the Surface Evolver program to analyze the stability of solder bridging for area array type packaging. Several factors that affect the stability of solder bridging spanning two identical circular pads are considered herein, including the pad size, the total volume of solder bumps, the pitch between adjacent pads, the contact angle between the molten solder alloy and the pad, the contact angle between the molten solder alloy and the solder mask and the surface tension of the molten solder alloy, respectively. The critical total volume of solder bumps and the critical pitch between adjacent pads are defined as the corresponding critical values to determine the solder bridging from a stable state to an unstable (vanishing) state. The stability of solder bridging spanning three and four identical circular pads is also discussed. Good agreement between the computed critical total volume of solder bumps for solder bridging and that available in the literature exhibits that the model developed in this work can be practically applied to predict the stability of solder bridging.

**keyword:** Solder Bump, Solder Bridging, Electronic Packaging, Surface Evolver Program

## 1 Introduction

Electronic packaging is incorporating ultra-fine-pitch technologies to meet the increasing demands for small scale, high density, rapid heat dissipation, high integration and superior quality in computers, communication systems, consumer electronic products and optoelectronic products. As seen in Fig. 1 [Chin, Khor, Sow, Ooi and Tan (2001)], solder bridging may be formed among adjacent terminals of electronic packaging. Furthermore, solder bridging may also be caused by inaccurate screen printing, improper solder placement, solder paste slumping, solder paste smearing, excessive solder paste volume, excessive rosin flux volume and incorrect reflow process, etc. Hence, solder bridging is a severe defect and has already attracted serious concern.

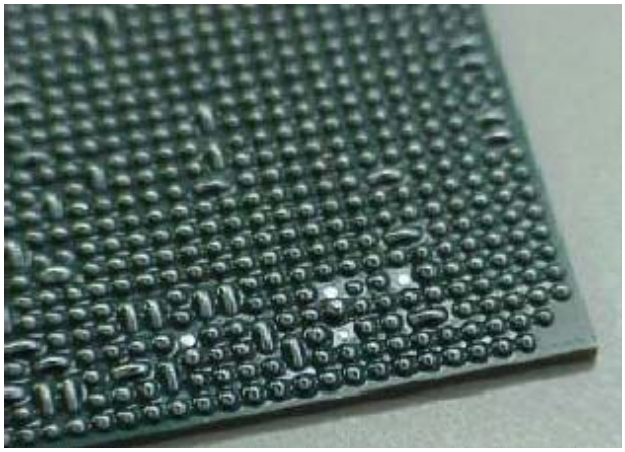

**Figure 1** : Solder bridging [Chin, Khor, Sow, Ooi and Tan (2001)]

Solder bridging is a complicated problem since it involves phase transformation, rapid liquid flow and the dynamic characteristics such as viscosity and inertia. However, this study only concerns the stability of solder bridging, that is, whether the solder bridging still exists when solidified ultimately rather than how the solder bridging is formed. Fortunately, the above dynamic characteristics exert only secondary influences on the shape and stability of solder bridging, since the characteristic time for readjustment and formation of a solder bridging is very rapid [Boettinger, Handwerker and Kattner (1993)]. Accordingly, surface tension is dominant in this problem, and solder bridging can be treated as an equilibrium capillary surface.

In the literature, liquid bridging between two parallel pads, which is the similar issue to solder bridging spanning two adjacent pads, has been studied extensively. Coriell, Hardy and Cordes (1977) employed the Laplace-

[1] Corresponding author, whchen@pme.nthu.edu.tw
[2] Department of Power Mechanical Engineering, National Tsing Hua University, Hsinchu, Taiwan 30013, Republic of China
[3] knchiang@pme.nthu.edu.tw

Young equation and minimum energy approach to explore the stability of a liquid zone between two parallel circular pads. Experiment is also performed by injecting a small water droplet into the zone between two coaxial rods using a micrometer syringe and then pulling down the lower rod to observe the stability of the liquid zone. Padday, Petre, Rusu, Gamero and Wozniak (1997) utilized the Laplace-Young equation and force balance to assess the shape of a pendant drop between two parallel circular endplate and then gradually increased the volume of the pendant drop until it became unstable and finally broke. The evaluated results were compared with those from experiments, which utilized a high speed video camera to record the bifurcation and breakage processes of the pendant pure water drop. Verges, Larson and Bacou (2001) undertook the similar investigations. Nagata, Kobayashi, Ogawa and Sakuta (2001) and Nagata, Kobayashi and Sakuta (2002) developed the rigid-plastic finite element method, which regarded molten solder as viscous fluid and incorporated the surface tension effect into the finite element analysis, to gauge the stability of pendant drop.

Glovatsky (1994) used mercury as the working fluid with two identical pads on substrate to simulate the stability of bridging spanning two identical pads. The different pad shapes, which were circular, rectangular and square, various pad sizes and varied separations were examined to identify the volumetric bridging stability. Although the surface tension of mercury is close to that of molten eutectic solder, the two liquids behave differently. Observing the stability of solder bridging spanning the pads is quite difficult through experiments, since the fluid flow of a solder bridging is very rapid. Hence, an analytical method needs be developed to assess the stability of solder bridging. Yamamoto, Lee, Shimokawa, Ishida and Soga (1995) printed solder paste onto a series of rectangular pads with a narrow solder channel connected to adjacent pads, and then reflowed the solder paste after mounting a Quad Flat Package (QFP) on the printed solder paste to observe the remaining number of solder bridgings to determine the impact of the pad size, the pitch between adjacent pads and solder materials on the solder bridging. Lee, Yamamoto, Shimokawa and Soga (1995) assumed that the geometry of solder bridging spanning two leads of QFP is arc-revolution. By evaluating the solder volume and minimizing the total energy, the shape of solder bridging spanning two leads of QFP can be outlined. By altering the solder volume, the minimal solder volume at which solder bridging is annihilated can be discovered. Cristini, Blawzdziewicz and Loewenberg (2001) presented an adaptive mesh algorithm on the evolving surface, which is described by a series of triangular facets to evaluate the drop breakup problems. The optimal configuration was achieved by minimizing the mesh energy through a sequence of local mesh restructuring. Furthermore, Chin, Khor, Sow, Ooi and Tan (2001) conducted numerous experiments by placing different amounts of flux and screen solder paste printing to form Ball Grid Array (BGA) solder joints with the reflow process to observe the influence of the quantity of flux on solder bridging.

The Surface Evolver program developed by Brakke (1992) is a general-purpose computer program, which interactively evolves the free surface of liquid drop toward the equilibrium shape, while minimizing the total energy associated with surface tension and other energies, such as the energy due to gravity. Moreover, the Surface Evolver program has been successfully adopted to predict the shape of the solder joints during the reflow process for various sizes and shapes of pads, volumes of solder joints and surface tensions [Chiang and Chen (1998); Li and Yeung (2001); Chen, Chiang and Lin (2002); Cheng, Yu and Chen (2005)]. Since the solder bridging can be treated as an equilibrium capillary surface, which is a static or quasi-static problem, the Surface Evolver program is appropriate for evaluating this problem. Whalley (1996) presented some preliminary results of the shape and stability of solder bridging spanning a group of rectangular pads using the Surface Evolver program. Singler, Zhang and Brakke (1996) applied the Surface Evolver program to explore the critical total volumes of solder bumps of the solder bridgings spanning two identical pads with circular, rectangular and square geometries. The shape of solder bridging spanning two circular pads was assumed to have two perpendicular symmetric planes, enabling a one-fourth model to be used. They also discussed the factors determining the stability of solder bridging. Li and Wang (2003) and Li, Bang, Kim, Wang and Zhang (2004) performed a similar work using QFP as the target packaging.

This study attempts to utilize the Surface Evolver program to simulate the stability of solder bridging. The solder bridging is supposed to have been formed already. In practice, as mentioned earlier, solder bridging is usu-

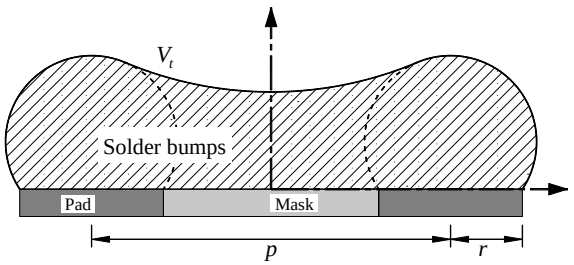


**Figure 2** : Schematic diagram of solder bridging spanning two identical circular pads

ally formed before and during the reflow process and this study therefore concerns about the stability of solder bridging after the reflow process. The model of two connected solder bumps spanning two identical circular pads is constructed first with a sufficiently large total volume of solder bumps, or a sufficiently small pitch between adjacent pads, to ensure that solder bridging is formed. The model adopted herein is a full model instead of a one-fourth model as adopted in Singler, Zhang and Brakke (1996). In general, because the real system is imperfectly symmetrical probably owing to the slight incline, soldering disproportion and manufacturing tolerance, the solder bridging separates into two unequal isolated solder bumps as it becomes unstable in such situation. The critical total volume of solder bumps of solder bridging is then defined as the critical (minimal) values of the total volume of solder bumps from a stable state to an unstable (vanishing) state. At the critical value, the total energy and the cross-section area at the middle section between adjacent pads suddenly jump down when the total volume of solder bumps is slightly disturbed. The critical total volume of solder bumps of the solder bridging obtained herein is also compared with the numerical data in the literature. Besides, this work also computes the critical pitch between adjacent pads of solder bridging to provide the packaging designer a suitable pitch between adjacent pads with other fixed parameters. Moreover, this investigation discusses the factors affecting the stability of solder bridging, including the pad size, the total volume of solder bumps, the pitch between adjacent pads, the contact angle between the molten eutectic solder and the pad, the contact angle between the molten eutectic solder and the solder mask, and the surface tension of the molten eutectic solder. Solder bridging models spanning a group of three or four identical circular pads are also established to examine the stability of solder bridging among a group of solder bumps.

## 2 Shape of Solder Bridging

Before using the Surface Evolver program to analyze the shape of solder bridging, the geometric parameters, illustrated in Fig. 2, are designated as follows.

$r$ radius of pad;

$p$ pitch between adjacent pads;

$V_t$ total volume of solder bumps;

Some fundamental assumptions are made to facilitate the analysis of the shape of solder bridging.

1. The impact of phase transformation is ignored.
2. The effect of viscosity and inertia of molten eutectic solder is disregarded.
3. The molten eutectic solder is considered not to permeate the solid surface.
4. The solder bumps are assumed to have reached static equilibrium prior to solidification.
5. The temperature is assumed to be maintained at the melting point, without temperature gradient exists inside the molten eutectic solder during the reflow process. Consequently, the variations of chemical potential and entropy and the change in volume due to thermal expansion are neglected, and the surface physical properties are fixed.
6. The pads are assumed to be wettable, but the surrounding solder mask is considered non-wettable. Therefore, the molten eutectic solder is assumed to spread completely over all of the pads but not to overflow onto the solder mask except in the zone between adjacent pads.
7. The contact angle between the molten eutectic solder and the solder mask is assumed to be constant.
8. The gravity effect is ignored since surface tension is much more dominant during solder bump reflow process.

The model for analyzing liquid shapes of multiple solder bumps is established first. All the volume of solder

bump placed on each pad is equal and the adjacent solder bumps are all connected with a solder bridging. The initial shapes of multiple solder bumps are described using a set of interconnected triangular surface facets. Initially, the model of multiple solder bumps usually has very simplistic and unrealistic shape, which is far from the configuration of equilibrium capillary surface. The model includes constraints such as: wettability condition between the molten eutectic solder and the pad or between the molten eutectic solder and the solder mask; volume constraint, namely the estimated total volume of solder bumps must equal the given value, and the boundary conditions, e.g. the molten eutectic solder cannot permeate a solid surface. Those constraints are involved in the model taken to be the particular level-set scalar function [Gary (1998)] of the vertex coordinates to restrict the degree of freedom of the vertices. The facets adopted in the computational model can be eliminated or refined during calculating, and the refined facets inherit the original constraints.

The total energy $E_t$ and the total volume of solder bumps $V_t$ are then estimated according to the surface facets of the initial shapes. The involved energy and volume can be written as

$$E_t = \sum_{i=1}^{m} \iint_{S_i^1} \gamma_l \, dA + \sum_{j=1}^{m} \iint_{S_j^2} \gamma_{sl}^p \, dA + \sum_{k=1}^{n} \iint_{S_k^3} \gamma_{sl}^m \, dA, \tag{1}$$

and

$$V_t = \sum_{i=1}^{m} \iiint_{\Omega_i} dV. \tag{2}$$

where $S_i^1$ is the $i$th region of the free surface of the molten eutectic solder, $S_j^2$ is the $j$th interfacial region between the molten eutectic solder and the pad, $S_k^3$ is the $k$th interfacial region between the molten eutectic solder and the solder mask, and $\Omega_i$ is the $i$th body domain of the molten eutectic solder; $\gamma_l$ is surface tension of the molten eutectic solder, $\gamma_{sl}^p$ is interfacial surface tension between the molten eutectic solder and the pad, $\gamma_{sl}^m$ is interfacial surface tension between the molten eutectic solder and the solder mask, $m$ is the number of pads, and $n$ is the number of regions between adjacent pads. The total energy $E_t$ can be expressed as a scalar function of all the vertex coordinates involving all the particular level-set scalar functions of constraints. Afterward, the free facets of the molten eutectic solder are then evolved towards the minimum total energy configuration.

## 3 Stability of Solder Bridging

It is emphasized that the critical total volume of solder bumps $V_c$ is adopted to distinguish the stable and unstable states of solder bridging, and the stage where the solder bridging proceeds from stable to unstable state is defined as the critical point. To calculate the critical total volume of solder bumps $V_c$ of the solder bridging spanning two identical circular pads, the model of two connected solder bumps spanning two identical circular pads is built first with a sufficiently large total volume of solder bumps $V_t$ to ensure that the solder bridging is formed. Then, the shape of solder bridging is estimated. Simultaneously, the Hessian matrix of the total energy $E_t$ [Brakke (1996)] is numerically computed. The Hessian Matrix computed herein is a positive definite matrix. By gradually decreasing the total volume of solder bumps $V_t$, the shape of solder bridging and the Hessian matrix of the total energy $E_t$ are computed in turn until the lowest eigenvalue of the Hessian matrix equals zero. At this stage, the bifurcation or catastrophe occurs [Gilmore (1981); Iooss and Joseph (1990)]. That is the total energy $E_t$ of solder bridging decreases suddenly with a small volume perturbation, and the solder bridging vanishes and separates into two isolated solder bumps. Thus, the total volume of solder bumps $V_t$ determined at this stage is the critical total volume of solder bumps $V_c$ of the solder bridging. The critical total volume of solder bumps $V_c$ of the solder bridging spanning three and four identical circular pads can be obtained similarly.

By the same token, the critical pitch $p_c$ between adjacent pads of solder bridging is the specific pitch $p$ between adjacent pads that distinguishes the stable and unstable states of solder bridging. Adjusting the total volume of solder bumps $V_t$ is easier than changing the pitch $p$ between adjacent pads when analyzing the shape of solder bridging using the Surface Evolver program. Hence, to calculate the critical pitch $p_c$ between adjacent pads of the solder bridging spanning two identical circular pads, the model of two connected solder bumps spanning two identical circular pads is constructed first with a sufficiently small pitch $p$ between adjacent pads to ensure that the solder bridging is formed. Then, bifurcation or catastrophe is induced by raising the pitch $p$ between adjacent pads and calculating the stability of the solder bridging

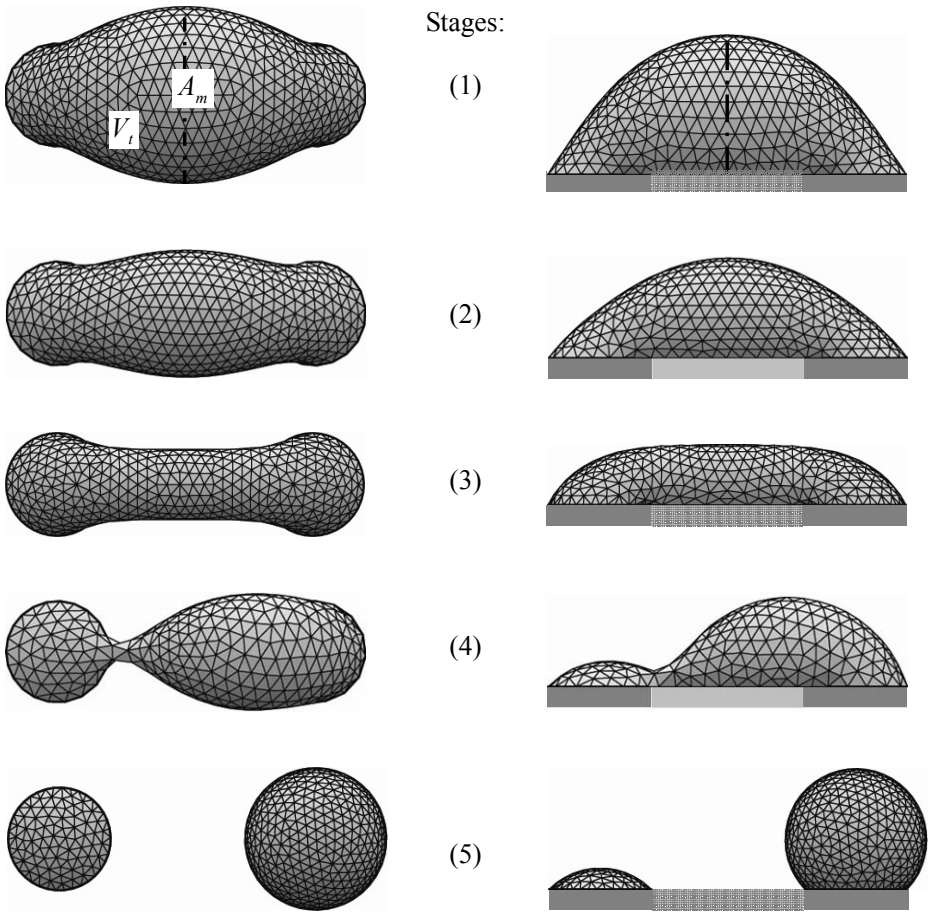


**Figure 3** : Stability of solder bridging versus the decrease of total volume of solder bumps

at the given total volume of solder bumps $V_t$ until the solder bridging becomes unstable or vanishing. The critical pitch $p_c$ between adjacent pads of the solder bridging spanning three and four identical circular pads can be found similarly.

## 4 Results and Discussions

In the following studies, except as specified, the radii of both pads are the same and equal to 0.1 *mm*; the surface tension $\gamma_l$ of the molten eutectic (Sn63%Pb37%) solder provided by Senju Metal Industry, Co., Ltd. is 48.1 *dyne/mm*; the contact angle between the molten eutectic solder and the pads, denoted as $\theta_c^p$ herein, is 11° [Liu and Tu (1998)], and the contact angle between the molten eutectic solder and the solder mask, denoted as $\theta_c^m$ herein, is 135° [Singler, Zhang and Brakke (1996)]. Furthermore, the pitch $p$ between adjacent pads is 0.5 *mm* in evaluating the critical total volume of solder bumps $V_c$ of solder bridging, while the total volume of solder bumps $V_t$ is $2.513 \cdot 10^{-2}$ $mm^3$ in calculating the critical pitch $p_c$ between adjacent pads of solder bridging.

Figure 3 shows a sequence of computational results of the shapes of the solder bridging spanning two identical circular pads with decreasing the total volumes of solder bumps $V_t$. The cross-section area $A_m$ at the middle section between adjacent pads is defined as in Fig. 3. To calculate the critical total volume of solder bumps $V_c$ of the solder bridging, the model of two connected solder bumps is built first with a large enough total volume of solder bumps $V_t$ to ensure that the solder bridging is

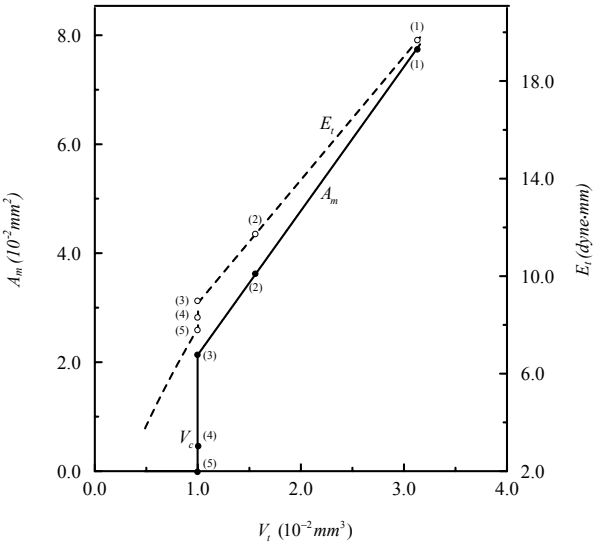


**Figure 4** : Variations of the cross-section area and total energy versus the decrease of total volume of solder bumps

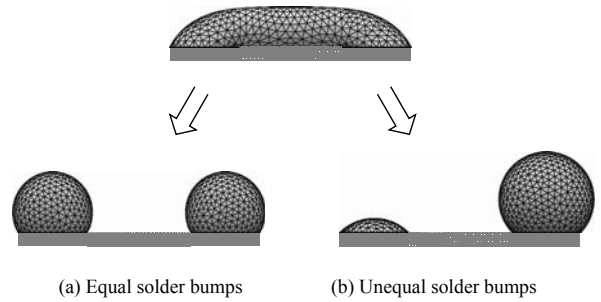


**Figure 5** : Possible situations at the critical point

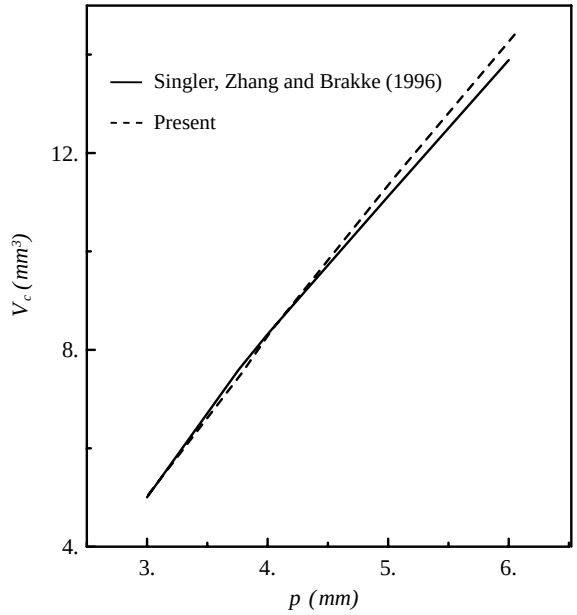


**Figure 6** : Variation of critical total volume of solder bumps versus different pitches

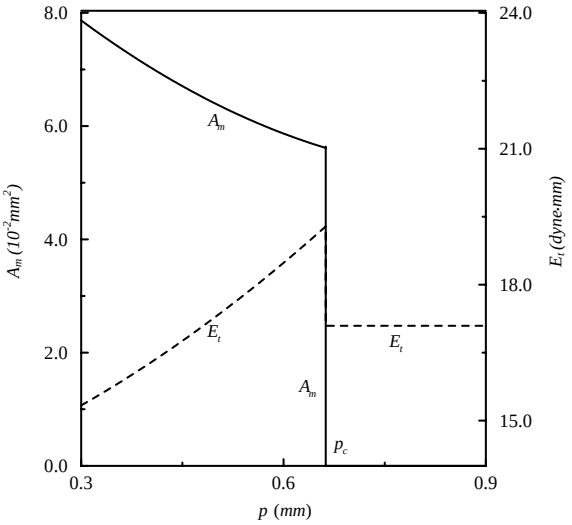


**Figure 7** : Variations of the cross-section area and total energy versus different pitches ($V_t = 2.513 \cdot 10^{-2}mm^3$)

formed. Then, the total energy $E_t$ and the cross-section area $A_m$ decrease with the decrease of the total volume of solder bumps $V_t$. The variations for various stages are displayed in Fig. 4. As shown in Figs. 3 and 4, the solder bridging initially shrinks as the total volume of solder bumps $V_t$ decreases, and then the lateral, and sometimes even the crest, of the solder bridging begins necking as the total volume of solder bumps $V_t$ continues to decrease. Eventually, the solder bridging vanishes and separates into two isolated solder bumps when the total volume of solder bumps $V_t$ is less than the critical total volume of solder bumps $V_c$, which equals $1.074 \cdot 10^{-2}$ $mm^3$ in this case. At the critical points (stages (3), (4) and (5)), the total energy $E_t$ and the cross-section area $A_m$

suddenly jump down. Notably, the higher critical total volume of solder bumps $V_c$ means that the solder bridging is more unstable and easier to vanish.

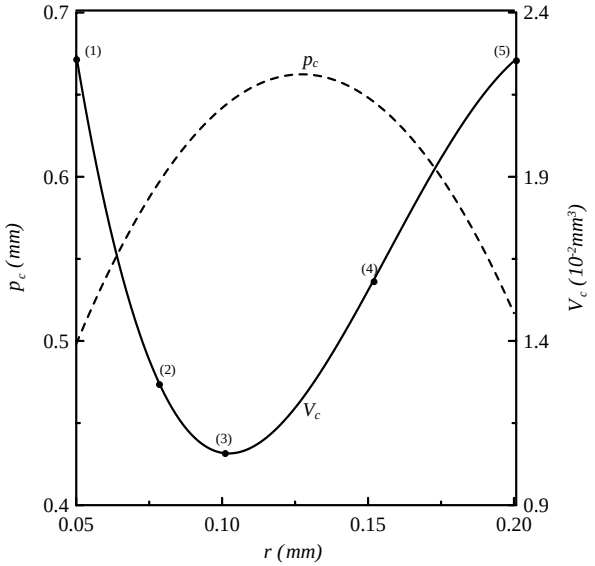


**Figure 12** : Variations of critical total volume of solder bumps and critical pitch versus different pad sizes

Significantly, if the solder bridging is perfectly symmetrical, then the solder bridging separates into two equal isolated solder bumps at the critical point, as shown in Fig. 5a. However, if the total volume of solder bumps $V_t$ is greater than that of the sphere with a radius equal to the radius of pad $r$, the solder bridging will separate into two unequal isolated solder bumps at the critical point as the system is imperfectly symmetrical. It is noted that, after mathematical analysis, the solder bumps have the least total surface area and, therefore, the minimum total energy $E_t$ when the radii of the two solder bumps are the same. As displayed in Fig. 5b, one of the two unequal isolated solder bumps is a monster solder bump approximated to a truncated sphere greater than the hemisphere and the other is a lean solder bump approximated to a truncated sphere smaller than the hemisphere. Moreover, if the total volume of solder bumps $V_t$ is smaller than that of the sphere with a radius equal to the radius of pad $r$, the solder bridging separates into two equal isolated solder bumps at the critical point no matter whether the system is perfectly symmetrical or not. In industry practice, however, extremely unequal isolated solder bumps often occur when a solder bridging spanns a group of three or more pads.

To verify the accuracy of the critical total volume of solder bumps $V_c$ of solder bridging obtained herein, as shown in Fig. 6, the present calculations of the critical total volume of solder bumps $V_c$ spanning two identical circular pads at different pitches are also compared with those available in the literature. For comparison purpose, the radii of both pads are equal to 1.245 *mm*. Excellent agreement exhibits that the computational model established herein can be used to predict the shape and stability of solder bridging accurately.

As seen in Fig. 7, the variations of total energy $E_t$ and the cross-section area $A_m$ at the middle section between adjacent pads of the solder bridging spanning two identical circular pads are evaluated with the increase of the pitch $p$. The calculated critical pitch $p_c$ between adjacent pads is depicted in Fig. 7. The total energy $E_t$ increases with the pitch $p$ due to the free surface of the solder bridging becomes larger, but the cross-section area $A_m$ has the opposite movement. Finally, the solder bridging separates into isolated solder bumps when the pitch $p$ arrives at the critical pitch $p_c$, which equals 0.641 *mm*. After being separated into two isolated solder bumps, the total energy $E_t$ suddenly jumps down and then remains constant value since the free surface area is now invariable, and the cross-section area $A_m$ drops to zero. Emphatically, the lower critical pitch $p_c$ between adjacent pads signifies that the solder bridging is more unstable and easier to vanish.

To elucidate the impact of physical properties of different solder alloys, such as the surface tension $\gamma_l$ of the molten solder, the contact angle between the molten solder and the pad $\theta_c^p$, and the contact angle between the molten solder and the solder mask $\theta_c^m$, on the stability of solder bridging, Figs. 8-10 illustrate the variations of the critical total volume of solder bumps $V_c$ and the critical pitch $p_c$. As seen in Fig. 8, the critical total volume of solder bumps $V_c$ and the critical pitch $p_c$ vary sensitively with the surface tension $\gamma_l$ of the molten solder alloy as the surface tension $\gamma_l$ is small, and gradually approach the constant values as the surface tension $\gamma_l$ of the molten solder alloy becomes large. Those phenomena demonstrate that the surface tension $\gamma_l$ of the molten solder alloy thus encourages the solder bridging to separate into isolated bumps when the surface tension $\gamma_l$ is large enough. Typically, the surface tension $\gamma_l$ of the molten solder alloy used in electronic packaging indus-

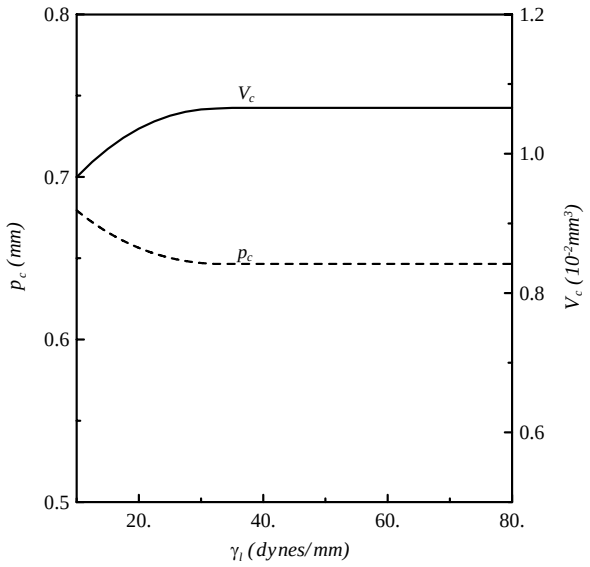


**Figure 8** : Variations of critical total volume of solder bumps and critical pitch versus different surface tensions

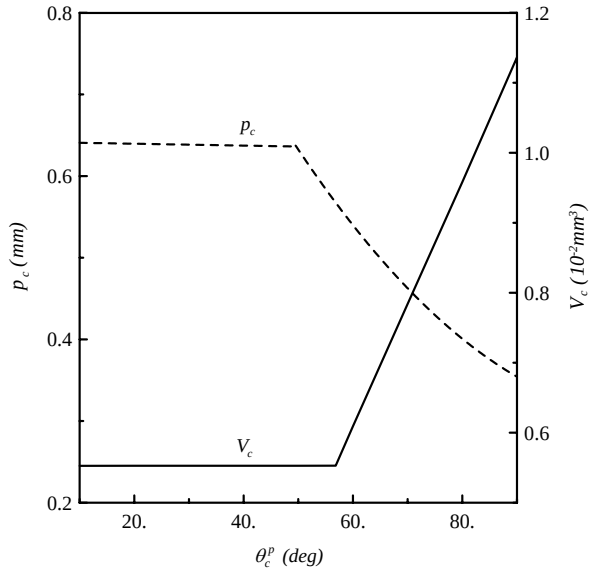


**Figure 9** : Variations of critical total volume of solder bumps and critical pitch versus different contact angles $\theta_c^p$

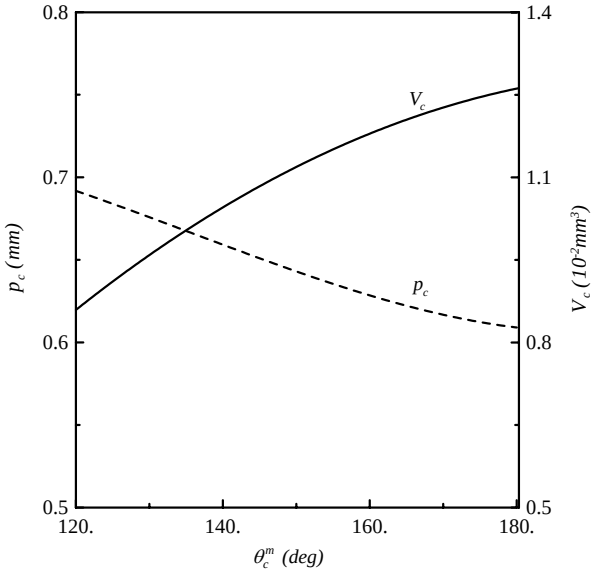


**Figure 10** : Variations of critical total volume of solder bumps and critical pitch versus different contact angles $\theta_c^m$

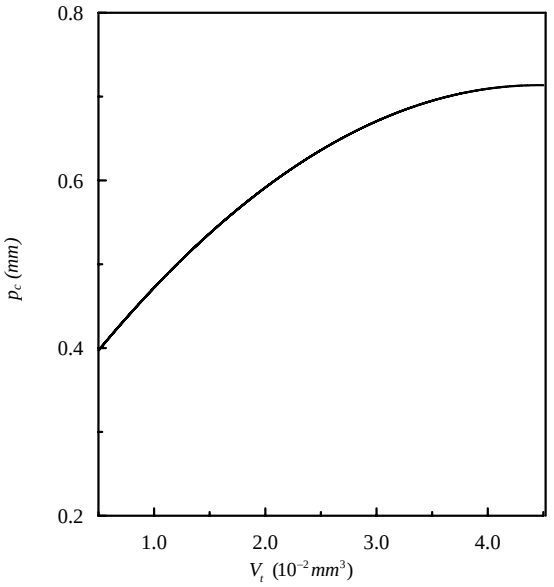


**Figure 11** : Variation of critical pitch versus different total volumes of solder bumps

try is about 30.0 *dynes/mm*, e.g. the surface tension $\gamma_l$ of the molten Sn42%Bi58% is 31.9 *dynes/mm* [Glazer (1994)], to 60.0 *dynes/mm*, e.g. the surface tension $\gamma_l$ of the molten pure Sn provided by Senju Metal Industry, Co., Ltd. is 57.4 *dynes/mm*. In such a region, the critical total volume of solder bumps $V_c$ and the critical pitch $p_c$ are insensitive to the alteration of the surface tension $\gamma_l$ of the molten solder. Figure 9 indicates that both the critical total volume of solder bumps $V_c$ and the critical pitch $p_c$ are almost stable when the contact angle $\theta_c^p$ is below $50^\circ$. This phenomenon is because the surface energy between the molten solder alloy and the pads can be treated

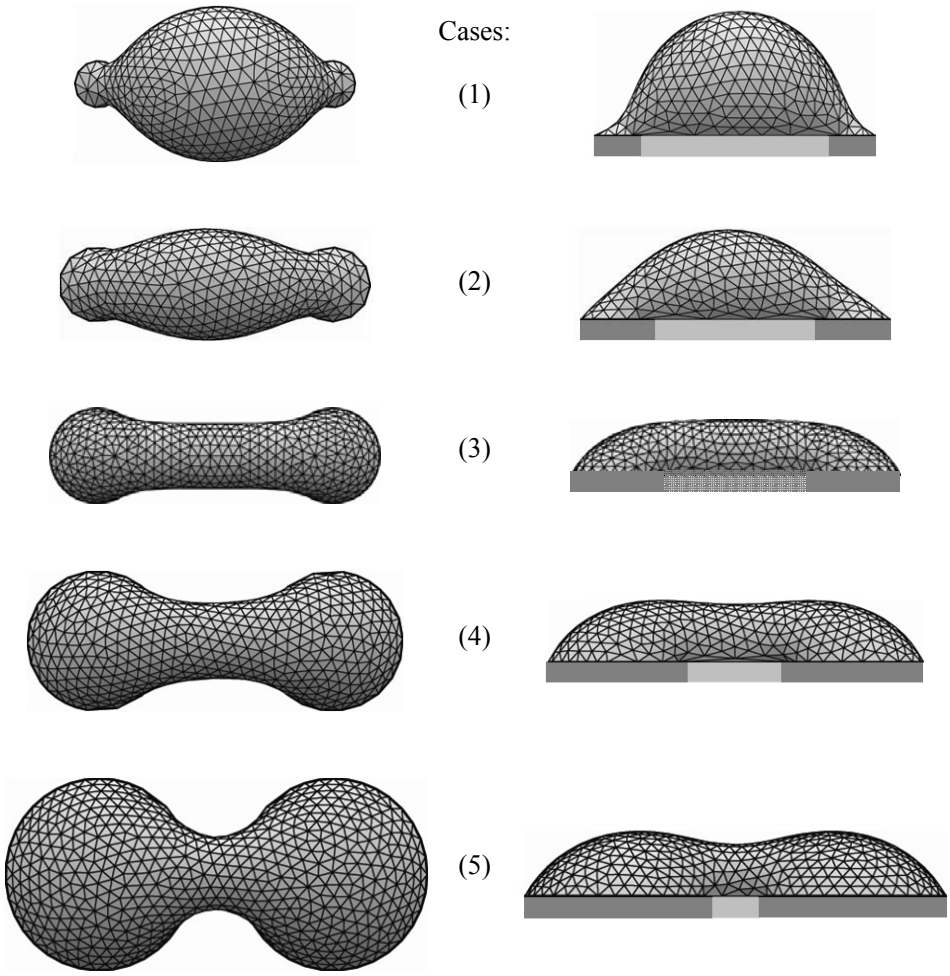


**Figure 13** : The solder bridgings at critical point with different pad sizes

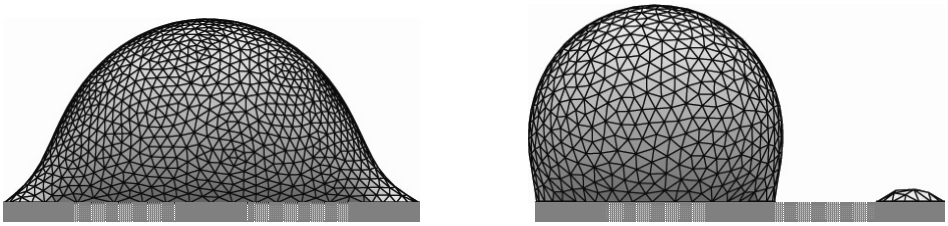

(a) Before first critical point (b) After first critical point

**Figure 14** : The solder bridging spanning three identical circular pads ($V_c^1 = 17.737 \cdot 10^{-2} mm^3$)

as constant during reflow process, since the molten solder alloy and the pads are well wettable and the interface area remains the same. When the contact angle $\theta_c^p$ is large, however, the wettability between the molten solder alloy and the pad is poor and more molten solder alloy is required to spread completely over the pad. Therefore, the critical total volume of solder bumps $V_c$ increases with the contact angle $\theta_c^p$, and the critical pitch $p_c$ decreases with the contact angle $\theta_c^p$. Significantly, when the contact angle $\theta_c^p$ is large, e.g. the molten solder alloy is oxidized, the solder is entirely dragged to a pad to create a large solder bump instead of separating into two isolated sol-

der bumps at the critical point. Figure 10 demonstrates that the critical total volume of solder bumps $V_c$ increases obviously with the contact angle $\theta_c^m$, while the critical pitch $p_c$ decreases. This is because the poor wettability between the molten solder alloy and solder mask destabilizes the solder bridging.

Figure 11 shows the influence of the total volume of solder bumps $V_t$ on the critical pitch $p_c$ between adjacent pads. As expected, the critical pitch $p_c$ increases with the total volume of solder bumps $V_t$. As the total volume of solder bumps $V_t$ is large enough, however, since the radius of pad $r$ is much smaller as compared to the total volume of solder bumps $V_t$ and the solder is constrained by the pads, the shape of solder bridging near the pads is abnormal. Consequently, the solder bridging will vanish near the pads and the value of critical pitch $p_c$ is therefore bounded.

To clarify the effect of radius of pad $r$ on the stability of solder bridging, Fig. 12 illustrates the comparison of critical total volume of solder bumps $V_c$ and the critical pitch $p_c$ between adjacent pads of solder bridging with different pad sizes. Generally, the molten solder alloy and the pads are well wettable, while the molten solder alloy and the solder mask are non-wettable. Therefore, with a constant pitch $p$ (0.5 $mm$), the critical total volume of solder bumps $V_c$ increases with the radius of pad $r$ when the pad is large, since the larger pad draws more molten solder toward the pad. However, the critical total volume of solder bumps $V_c$ decreases with the radius of pad $r$ while the pad is small, since the smaller pad leaves more molten solder at the middle region between the adjacent pads and the solder bridging will vanish near the pads. In addition, with a constant total volume of solder bumps $V_t$ ($2.513 \cdot 10^{-2}\, mm^3$), the tendency of the critical pitch $p_c$ is in contrast with the critical total volume of solder bumps $V_c$. Referring to Fig. 12, several cases of solder bridging at critical point with different pad sizes and critical total volumes of solder bumps $V_c$ under a constant pitch $p$ are displayed in Fig. 13.

To calculate the stability of solder bridging spanning three and four identical circular pads, the models of three and four connected solder bumps with identical circular pads arranged in a row are constructed and denoted as models A and B, respectively. The model of four connected solder bumps where the pads are arranged in an area array $(2 \times 2)$ is also built and denoted as model C. By repeating the similar process as in calculating the solder bridging spanning two identical circular pads, the critical total volume of solder bumps $V_c$ and the critical pitch $p_c$ between adjacent pads of the solder bridging spanning three and four identical circular pads can be obtained. Tables 1 and 2 list the critical total volume of solder bumps $V_c$ and the critical pitch $p_c$ of the solder bridging of models A-C. The critical total volume of solder bumps $V_c$ and the critical pitch $p_c$ of the solder bridging spanning three identical circular pads have two critical values, while those of solder bridging spanning four identical circular pads have three critical values. All the distinct values are distinguished by superscripts. Referring to Tables 1 and 2, as predicted, the solder bridging spanning three and four identical circular pads arranged in a row is much unstable than the solder bridging spanning two identical circular pads, for which $V_c = 1.074 \cdot 10^{-2} mm^3$ and $p_c = 0.641 mm$. Furthermore, the computational results also indicate that the solder bridging spanning in area array type pads is more stable than the solder bridging spanning the pads in a row before the first and second critical points. Figure 14 shows an example of the stability of solder bridging of model A spanning three pads before and after the first critical point.

## 5 Concluding Remarks

The stability of solder bridging has been successfully investigated in this work using the Surface Evolver program. The effects of various design factors, including the pad size, the total volume of solder bumps, the pitch between adjacent pads, the contact angle between the molten solder alloy and the pad, the contact angle between the molten solder alloy and the solder mask and the surface tension of the molten solder alloy are studied in details based on the proposed model. The critical total volume of solder bumps of solder bridging obtained in this work is in excellent agreement with that in the literature.

The results reveal that the solder bridging becomes unstable when the radius of pad is small enough under constant pitch and total volume of solder bumps. In addition, for the general solder alloy used in industry, the stability of solder bridging is insensitive to the surface tension of molten solder alloy and the contact angle between the molten solder alloy and the pad, but is sensitive to the contact angle between the molten solder alloy and the solder mask.

Since the solder bridging is usually formed before and

| | $V_c^1(10^{-2}mm^3)$ | $V_c^2(10^{-2}mm^3)$ | $V_c^3(10^{-2}mm^3)$ |
|---|---|---|---|
| Model A | 17.737 | 1.134 | - |
| Model B | 91.511 | 17.048 | 1.102 |
| Model C | 5.050 | 5.030 | 1.138 |

**Table 1** : The critical total volume of solder bumps $V_c$ of the solder bridging spanning three and four identical circular pads

| | $p_c^1$(mm) | $p_c^2$(mm) | $p_c^3$(mm) |
|---|---|---|---|
| Model A | 0.349 | 0.687 | - |
| Model B | 0.248 | 0.376 | 0.747 |
| Model C | 0.503 | 0.503 | 0.738 |

**Table 2** : The critical pitch between adjacent pads $p_c$ of the solder bridging spanning three and four identical circular pads

during the reflow process in practice, the solder bridging studied in this work is supposed to have been formed already. However, to promote the solder joint density required for ultra-fine-pitch technologies, the occurrence of solder bridging before and during the reflow process should be avoided. Then, the solder flux placing and heat convection need be considered in the computational model. To deal with such problems, the meshless finite volume method [Atluri, Han and Rajendran (2004)] may be an appropriate approach, and will be attempted in future work.

**Acknowledgement:** The authors would like to thank the National Science Council of the Republic of China for the financial support under Contracts NSC-90-2212-E-007-051 and NSC-91-2212-E-007-052. The authors' appreciation is also conveyed to Prof. Kenneth A. Brakke, Susquehanna University, for his numerous useful discussions regarding the Surface Evolver Program.

## References

**Atluri, S. N.; Han, Z. D.; Rajendran, A. M.** (2004): A New Implementation of the Meshless Finite Volume Method, Through the MLPG "Mixed" Approach. CMES: *Computer Modeling in Engineering & Sciences*, vol. 6, no. 6, pp. 491-513

**Boettinger, W. J.; Handwerker, C. A.; Kattner, U. R.** (1993): *The Mechanics of Solder Alloy Wetting and Spreading*. Van Nostrand Reinhold, New York, Chap. 4.

**Brakke, K. A.** (1992): The Surface Evolver. *Experimental Mathematics*, vol. 1, no. 2 pp. 141-165.

**Brakke, K. A.** (1996): The Surface Evolver and the Stability of Liquid Surfaces. *Philosophical Transactions of the Royal Society of London, Ser.A*, vol. 354, pp. 2143-2157.

**Chen, W. H.; Chiang, K. N.; Lin, S. R.** (2002): Prediction of Liquid Formation for Solder and Non-Solder Mask Defined Array Packages. *ASME Journal of Electronic Packaging*, vol. 124, pp. 37-44.

**Cheng, H. C.; Yu, C. Y.; Chen, W. H.** (2005): An Effective Thermal-mechanical Modeling Methodology for Large-scale Area Array Typed Packages. CMES: *Computer Modeling in Engineering & Sciences*, vol. 7, no. 1, pp. 1-17.

**Chiang, K. N.; Chen, W. L.** (1998): Electronic Packaging Reflow Shape Prediction for the Solder Mask Defined Ball Grid Array. *ASME Journal of Electronic Packaging*, vol. 120, no. 2, pp. 175-178.

**Chin, Y. T.; Khor, C. K.; Sow, H. P.; Ooi S. J.; Tan, H. B.** (2001): Breakthrough Ball Attach Technology by Introducing Solder Paste Screen Printing. *Proc. 51st IEEE Electronic Components and Technology Conference*, Orlando, Florida, USA, pp. 198-202.

**Coriell, S. R.; Hardy, S. C.; Cordes, M. R.** (1977): Stability of Liquid Zones. *Journal of Colloid and Interface Science*, vol. 60, no. 1, pp. 126-136.

**Cristini, V.; Blawzdziewicz, J.; Loewenberg, M.** (2001): An Adaptive Mesh Algorithm for Evolving Surfaces: Simulations of Drop Breakup and Coalescence. *Journal of Computational Physics*, vol. 168, pp. 445-463.

**Gary, A.** (1998): *Modern differential geometry of curves and surfaces with Mathematica*. Boca Raton, FL: CRC Press, Chap.12.

**Gilmore, R.** (1981): *Catastrophe Theory for Scientists and Engineers*. John Wiley & Sons, Inc., New York.

**Glazer, J.** (1994): Microstructure and mechanical properties of Pb-free solder alloys for low-cost electronic assembly. *Journal of Electronics Materials*, vol. 23, no. 8, pp. 693-700.

**Glovatsky, A. Z.** (1994): *An Experimental Investigation of the Stability of Simulated Solder Bridges*. Master Thesis, Department of Science in Mechanical Engineering, The State University of New York, Binghamton.

**Iooss, G.; Joseph, D. D.** (1990): *Elementary Stability and Bifurcation Theory*. 2nd eds. Springer-Verlag, New York.

**Lee, C.; Yamamoto, K.; Shimokawa, H.; Soga, T.** (1995): The Analysis on Bridge between Leads of Quad Flat Package in Reflow Soldering on Printed Circuit Boards. *Proc. 18th IEEE/CPMT IEMT Symposium*, Omiya, Japan, pp. 411-414.

**Li, L.; Yeung, B. H.** (2001): Wafer Level and Flip Chip Design through Solder Prediction Models and Validation. *IEEE Transaction on Components and Packaging Technologies*, vol. 24, no. 4, pp. 650-654.

**Li, M. Y.; Wang, C. Q.** (2003): Solder Joint Design Attribute to No Solder Bridge for Fine Pitch Device. *Proc. 5th IEEE ICEPT*, Shanghai, China, pp. 70-75.

**Li, M. Y.; Bang, B. S.; Kim, Y. P.; Wang, C. Q.; Zhang, L.** (2004): Simulative Analysis on Factors Influencing Solder Joint Bridging of Fine Pitch Devices. *ASME Journal of Electronic Packaging*, vol. 126, no. 1, pp. 22-25.

**Liu, C. Y.; Tu K. N.** (1998): Morphology of Wetting Reactions of SnPb Alloys on Cu as a Function of Alloy Composition. *Journal of Material Research*, vol. 13, no. 1, pp. 37-44.

**Nagata, T.; Kobayashi, T.; Ogawa, K.; Sakuta, H.** (2001): Prediction of Solder Joint Geometries by Rigid-plastic Flow Analysis. *ASME IPACK'01*, Kauai, Hawaii, USA, pp. 1255-1260.

**Nagata, T.; Kobayashi, T.; Sakuta, H.** (2002): Prediction of Equilibrium and Stability of Molten Solder Profiles by Finite Element Analysis. *ASME IMECE'02*, New Orleans, Louisiana, pp. 361-368.

**Padday, J. F.; Petre, G.; Rusu, C. G.; Gamero, J.; Wozniak, G.** (1997): Shape, Stability and Breakage of Pendant Liquid Bridges. *Journal of Fluid Mechanics*, vol. 352, pp. 177-204.

**Singler, T. J.; Zhang, X.; Brakke, K. A.** (1996): Computer Simulation of Solder Bridging Phenomena. *ASME Journal of Electronic Packaging*, vol. 118, no. 3, pp. 122-126.

**Verges, M. A.; Larson, M. C.; Bacou, R.** (2001): Force and Shapes of Liquid Bridges between Circular Pads. *Experimental Mechanics*, vol. 41, no. 4, pp. 351-357.

**Whalley, D. C.** (1996): A Model to Explain SMT Open Circuit Joints Associated with Adjacent Solder Bridges. *Journal of Electronics Manufacturing*, vol. 6, no. 1, pp. 39-44.

**Yamamoto, K.; Lee, C.; Shimokawa, H.; Ishida, T.; Soga, T.** (1995): Development of Sn-Pb-Bi Solder Materials for Fine Pitch Package. *Proc. 18th IEEE/CPMT IEMT Symposium*, Omiya, Japan, pp. 232-235.